FOREX Publication
Open Access | Rapid and quality publishing

International Journal of
Electrical and Electronics Research (IJEER)
Research Article | Volume 13, Issue 4 | Pages 772-783 | e-ISSN: 2347-470X

An Effective Dual-Band Wireless Power Transfer (WPT) System using Transmission Line Equivalents for Medical Implants

Nuha H. Abdulghafoor[1*], and Zainab N. Abbas[2]

[1]Department of Electronic Engineering, College of Electrical Engineering, University of Technology- Iraq, Baghdad, Iraq; Email: nuha.h.abdulghafoor@uotechnology.edu.iq
[2]Department of Electrical Engineering, College of Electrical Engineering, University of Technology- Iraq, Baghdad, Iraq; Email: zainab.n.abbas@uotechnology.edu.iq

***Correspondence:** *Nuha H. Abdulghafoor; Email: nuha.h.abdulghafoor@uotechnology.edu.iq; Tel. 009647702773504*

ABSTRACT- There has been a pressing need for wireless power transfer due to its numerous applications, including integrated or embedded systems used in various fields, such as sensors and mobile devices, as well as medical devices implanted inside the human body. Traditional transmission methods have drawbacks in terms of protection and safety when used directly on the human body, as well as the requirement for continuous operation within the body. Therefore, wireless power transfer methods have emerged as a safe and reliable alternative, especially for medical implants. Several methods and techniques have been developed, initially operating on a single frequency. This has since been developed to utilize dual-band or dual-frequency systems, making them more adaptable to changing environments and enabling simultaneous power transmission and information exchange between the implant inside the body and the external component of the wireless power transfer system. This article presents an efficient dual-band wireless power transfer system for use in building multifunctional systems. It also demonstrates the compatibility between the operating and load circuits. It also features a reduction in energy losses resulting from unwanted mutual induction caused by the large number of inductive coils, whether on the supply side or the load side, which in turn enhances the efficiency of energy transfer sent and received by the load circuit located inside the human body, which reached approximately 60%, the values of reflection loss were reduced to a suitable level approaching 0 dB.

Keywords: Wireless Power Transfer, Dual-Band, Resonant, Inductive Coupling, Implant Medical Application.

ARTICLE INFORMATION
Author(s): Nuha H. Abdulghafoor, and Zainab N. Abbas;
Received: 13/07/2025; **Accepted:** 24/11/2025; **Published:** 15/12/2025;
E- ISSN: 2347-470X;
Paper Id: IJEER 1307-09;
Citation: 10.37391/ijeer.130417
Webpage-link:
https://ijeer.forexjournal.co.in/archive/volume-13/ijeer-130317.html

Publisher's Note: FOREX Publication stays neutral with regard to jurisdictional claims in Published maps and institutional affiliations.

1. INTRODUCTION

Wireless Power Transfer (WPT) showed great effective in several devices, including sensors, medical implants, and mobiles. Medical applications underscore the critical needed for safe and dependable wireless power to overcome the constraints associated with implanted batteries. Initially proposed by Nikola Tesla [1], WPT technology has obedience to the commands substantial advancements and is presently employed across a multitude of applications, including electric vehicles and drones [2-3]. WPT systems are typically categorized into two distinct types: near-field and far-field, and they impact technologies such as inductive coupling, magnetic resonance, and radio frequency (RF)/microwave transmission [4]. International standards have been established for various frequencies to facilitate contemporary wireless charging, exemplified by the Wireless Power Consortium (A4WP), which operates at 6.78 MHz, and the Industrial, Scientific, and Medical (ISM) standard, which employs 13.56 MHz.

To address this issue, multiband WPT systems have emerged, as shown in *figure 1*. These systems allow simultaneous charging of devices operating at different frequencies, improving compatibility, efficiency, and safety, while still meeting power transfer and electromagnetic safety limits. These systems are used in a variety of applications, including biomedical devices, telemedicine, wireless sensors, and automotive charging [5]. Many dual-band wireless power transfer (WPT) system designs have been explored [7-9] to improve efficiency, reduce crosstalk, and simplify implementation, such as multi-coil configurations. However, these designs have encountered problems, including high manufacturing complexity and frequency mismatches. Although they had issues at higher frequencies, single-coil, double-resonant designs decreased coupling. Although they were frequently heavy or unfeasible, solutions like repeaters and 3D wire structures increased performance. Nevertheless, single-coil, double-resonant designs minimized the coupling but were plagued at higher frequencies. Repeater and 3D wire structures improved performance but often could be cumbersome or impracticable. This paper describes a dual-resonant single-coil transceiver using external discrete coils as matching networks being implemented on an PCB to enhance compactness and precision. This enables it to

FOREX Publication
Open Access | Rapid and quality publishing
International Journal of Electrical and Electronics Research (IJEER)
Research Article | Volume 13, Issue 4 | Pages 772-783 | e-ISSN: 2347-470X

operate effectively in two frequency bands: 6.78 and 13.56 MHz. This paper describes a part of the design of a dual-resonant single-coil transceiver that uses an external discrete coil as matching networks. The key parameters in view that made the impedance match across the dual bands possible are the inductances of the external coils and their coupling coefficients with the internal resonators. The resonant frequency of choice for the system is set as 6.78 MHz and 13.56 MHz [8].

A dual-band device for efficient wireless power transfer [9-10] is addressed the challenges of dual-band and single-coil wireless power transmission systems, including the difficulty of achieving high power transmission efficiency at both operating frequencies simultaneously. To address this challenge, the paper [11] is proposed integrating a repeater into the coil unit [11]. It helped in balance the efficiency difference between the two frequencies by improving the low power transfer efficiency at the lower frequency (6.78 MHz). Simulation results showed that using a repeater increases the average power transfer coefficient at both frequencies (6.78 MHz and 13.56 MHz), thus improving the overall power transmission performance for fast charging in mobile devices. Study [12] presents a technique for integrating bidirectional data communication into a wireless power transmission system using a single-coil and dual-resonant architecture simultaneously. The researchers developed a proposed two-channel transmission model that supports simultaneous wireless power and information transmission. The research also demonstrated improved communication performance under misaligned coils. Simulations and experiments have confirmed the validity of this approach, providing a system for transmitting up to 354 watts of power and 19.2 kilobits per second of data across a one-meter air gap.

The paper [13] presents a dual-band wireless power transfer (WPT) architecture that operates efficiently at two different frequencies, enabling compatibility with a wide range of applications, from high-power systems (100 kHz) to compact, misalignment-tolerant systems (13.56 MHz). A reconfigurable dual-band rectifier is implemented on the receiver side, achieving high power density (400 W/in³) and operating effectively at both frequencies with a minimal component count. The system can operate under significant coil misalignment and varying load conditions. The paper [14] presents a dual-band wireless power transfer (DWPT) system capable of delivering more power and supporting higher data rates than traditional single-band systems, all within the limits of electromagnetic fields. The paper presents analytical studies on the effect of source and load inductance on impedance matching, derives the voltage transfer function, and defines the conditions for optimal power transfer. The experimental results confirm power transfer efficiencies of 71% at 6.78 MHz and 56% at 13.56 MHz [14]. A dual-resonant single-coil design minimizes frequency crosstalk and serves as both a transmitter and a receiver [15]. The primary design challenge—achieving impedance matching at two resonant frequencies—is addressed by adjusting the coupling factor between the source and load, as well as the dual-band resonator. The main contributions of this manuscript are the use of transmission-line-based equivalent models instead of conventional lumped elements to achieve dual-resonant operation (6.78 MHz & 13.56 MHz) with reduced coupling losses and a smaller WPT circuit size.

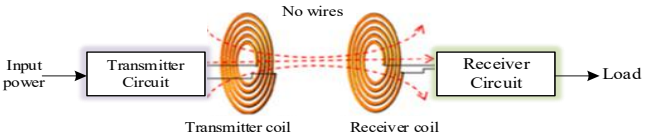

Figure 1. Wireless Power Transfer System Diagram

2. METHODOLOGY

To design and analysis of the operation of a dual-band coil, the equivalent circuit of the dual-band coil [8] includes an Lumped Component (LC) branch (a lumped capacitor in series with the coil) and an LC tank (a lumped capacitor in parallel with a lumped inductor) by which two resonant frequencies can be obtained as shown in *fig. 2*, The LC tank either behaves inductively when its operating frequency is lower than its resonant frequency or behaves capacitive when its operating frequency is higher than its resonant frequency. It indicates that an LC tank can be considered as an inductor or a capacitor outside its resonant frequency. Therefore, the lower dual-band resonant frequency is obtained by combining an LC branch with the inductive LC tank in series. On the other hand, the higher dual-band resonant frequency can be obtained by combining an LC branch with the capacitive LC tank in series [8]. The resonant frequencies can be expressed as:

$$f_{r1} = \frac{1}{2\pi\sqrt{(L_1+L_2)C_1}} \quad (1)$$

$$f_{r2} = \frac{1}{2\pi\sqrt{L_1(C_1||C_2)}} \quad (2)$$

The equivalent impedance of this dual-band coil can be expressed as;

$$Z_{in} = Z_p + j\omega L_1 + \frac{1}{j\omega C_1} + \left(j\omega L_2 \,/\!/\, \frac{1}{j\omega C_2}\right) \quad (3)$$

Where Z_p denotes the total parasitic resistance of the coil and lumped inductor [8], which can be neglected when parasitic resistance is small.

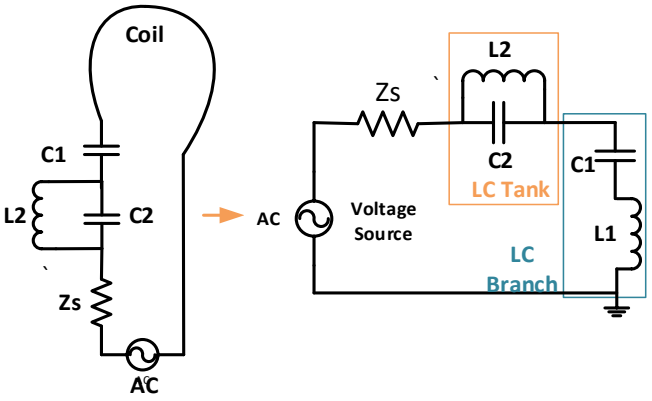

Figure 2. Dual-Band Coil Driver and its equivalent model [7]

The dual-band coil module for applying to WPT systems is obtained by combining the presented dual-band coils. This coil

FOREX Publication
Open Access | Rapid and quality publishing
International Journal of Electrical and Electronics Research (IJEER)
Research Article | Volume 13, Issue 4 | Pages 772-783 | e-ISSN: 2347-470X

module is analyzed in detail using two critical concepts: impedance matching [8, 16] and power transmission efficiency (PTE). A WPT two-port network comprises the power source and power driver at the source end, the rectifier, and receiving loads at the load end [7-8]. The Thevenin equivalent circuit consists of the power driver and power source; the rectifier and receiving loads are comparable to a single load. A schematic diagram of a dual-band WPT system is shown in *fig. 3(a)*, which is equivalent to the circuit model in *fig. 3(b)*.

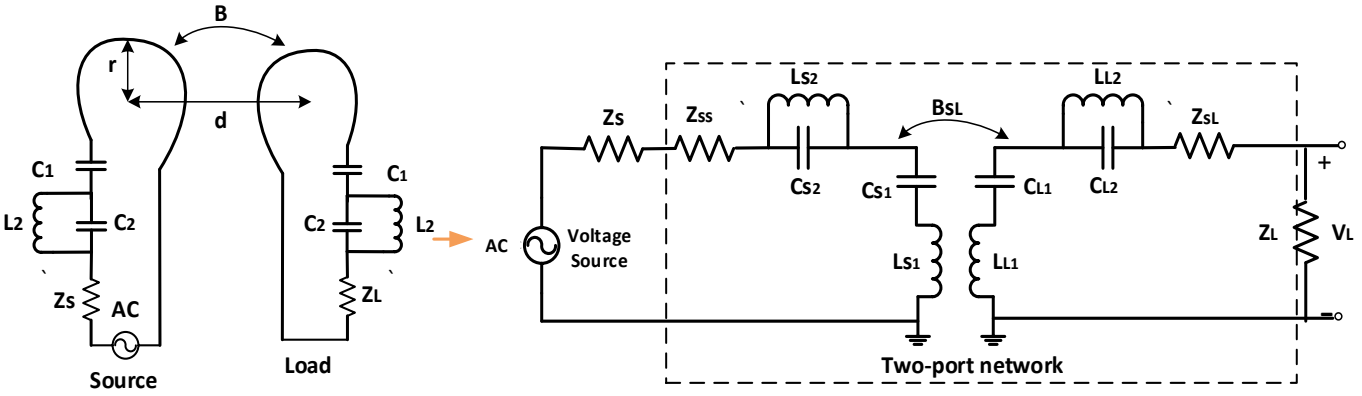

Figure 3. Dual-Band WPT Two-port Network [7]

The input and total impedance of source and load equivalent models can be expressed as shown:

$$Z_{ins} = Z_s + j\omega L_{s1} + \frac{1}{j\omega C_{s1}} + (j\omega L_{s2} || \frac{1}{j\omega C_{s2}}) \quad (4)$$

$$Z_{inL} = Z_L + j\omega L_{L1} + \frac{1}{j\omega C_{L1}} + (j\omega L_{L2} || \frac{1}{j\omega C_{L2}}) \quad (5)$$

The forward transmission coefficient (S21) and the PTE of the Dual-Band WPT two-port model are expressed as follows [8]:

$$S_{21} = \frac{2\sqrt{Z_s}}{\sqrt{Z_L}} \cdot \frac{V_L}{V_s} = \frac{2Z_s\sqrt{r_z}\omega_r M_{SL}}{r_z Z_s^2 + \omega_r^2 M_{SL}^2} \quad (6)$$

$$\eta_{coil} = |S_{21}|^2 \quad (7)$$

Where ω_r is the resonance frequency in radians,

$$r_z = Z_L/Z_s \quad (8)$$

$$M_{SL} = Z_s\sqrt{r_z} \quad (9)$$

According to *figure 4*, which shows the flowchart of the design WPT, the first step is to determine the basic specifications, such as target frequencies (6.78 and 13.56 MHz), delivered power, Tx/Rx geometry, *etc.* Then design the Lumped/Transmission-line component and calculate its initial value using the previous equation. After that, simulate the proposed circuit using a suitable simulation tool, such as Advanced Design System (ADS). The next step includes sweep components for impedance matching and the calculation of performance parameters, such as Scatter Parameters (SP) and Power Transfer Efficiency. The 3D EM coil simulation generates a 3D geometry of a dual-band coil module and Tx/Rx with tissue/implant load. Finally, draw the necessary parameters, such as S21, PTE, delivered power *vs.* distance/misalignment, and SAR, for safety and regulatory purposes.

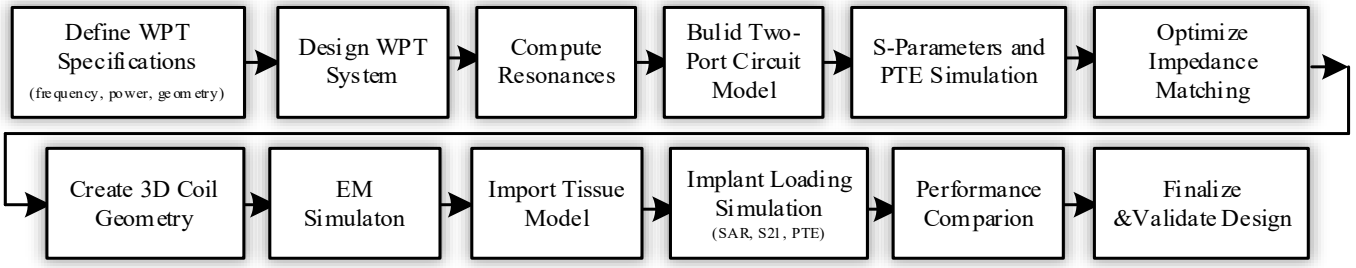

Figure 4. Dual-Band WPT Methodology Block Diagram

FOREX Publication
Open Access | Rapid and quality publishing
International Journal of Electrical and Electronics Research (IJEER)
Research Article | Volume 13, Issue 4 | Pages 772-783 | e-ISSN: 2347-470X

3. THE PROPOSED EQUIVALENT WPT SYSTEM DESIGN

Inductors and capacitors are grouped elements that store energy in static magnetic and electrostatic fields, respectively. These elements offer wide frequency ranges but are primarily limited by parasitic effects, which can be minimized through careful design and optimization. Where high frequencies are required in some applications, inductors are made smaller to reduce their intrinsic capacitance and limit their maximum no-load capacity [17]. In contrast, transmission lines are distributed elements that store energy in both static magnetic and electrostatic fields, making them an ideal alternative to inductors and capacitors. These lines are designed as interconnected networks of series-connected inductors and parallel-connected capacitors. Short sections of transmission lines can mimic the behavior of inductors or capacitors, depending on their length, terminals, and impedance. Larger distributed elements can store more energy with relatively lower losses, thus increasing their no-load capacity, although modulation limits their size. Multiple equivalents exist between distributed components, enabling the design of diverse electronic circuits, such as wireless power transfer devices and filters, by determining the cutoff frequency (also known as the center frequency), the angular frequency, and the quality factor (Q) as criteria for the quality of these designs [18]. In this research, two cases of assembled components (LC) and their equivalent transmission lines (TL) were used, as shown in *table 1*.

Initially, only the drive circuit was designed, as shown in the *figure 5*, where two models were proposed based on the two cases above. The component values were calculated using the equations mentioned in the previous section and summarized in *table 2* for the two hybrid assembled components (LC) and transmission lines (TL) models (Model 1 and Model 2). Model 1 replaces the inductor in the tank section with its corresponding transmission line. Model 2 eliminates certain LC components (L_2, C_2) and replaces them with TL sections, thus simplifying the physical implementation while maintaining performance. Two cases(case 1 and case 2) are proposed, each with a different inductance ratio (r_L) . These models were subsequently tested, and their results were presented and compared with previous designs [7-8], as shown in the Experimental Results Simulation section. This dual-band coil unit does not exhibit the unwanted mutual electromagnetic interference typical of multi-coil wireless power transmission systems because it contains only two coils and distributed elements dependent on the transmission lines, which provide the necessary electromagnetic power transmission. The inductances grouped within the coil are relatively small. Each inductor has its own axis, which is perpendicular to the coil axis, allowing mutual coupling between the grouped inductors and the coils to be neglected [8]. Consequently, the total mutual inductance between the two coils is zero. Therefore, two complete power transmission system models (Model 1 and Model 2), consisting of a driver and a load circuits, were proposed, as shown in *figure 6*. The values of their respective components are specified in *table 3*. Distributed line elements were used as replacements for bundled elements to reduce internal coupling losses when more than two coils are present in the wireless power transmission system, and to increase the power received by the load or implanted device. The effect of impedance matching on the power transmission system was investigated (Case 3 and Case 4), where Case 3 represents impedance mismatch and Case 4 represents impedance matching. These two cases were tested and analyzed, as described in the following section.

Table 1. Lumped and distributed transmission line component equivalent models

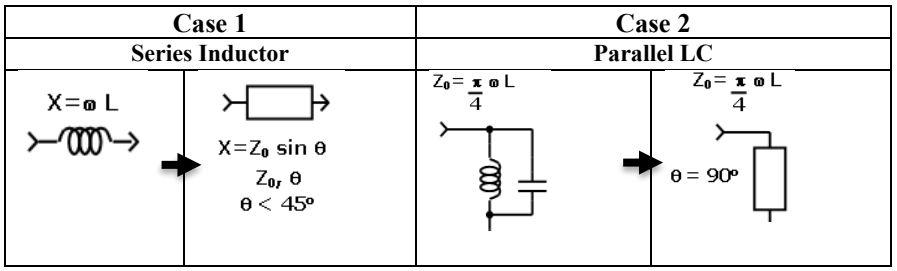

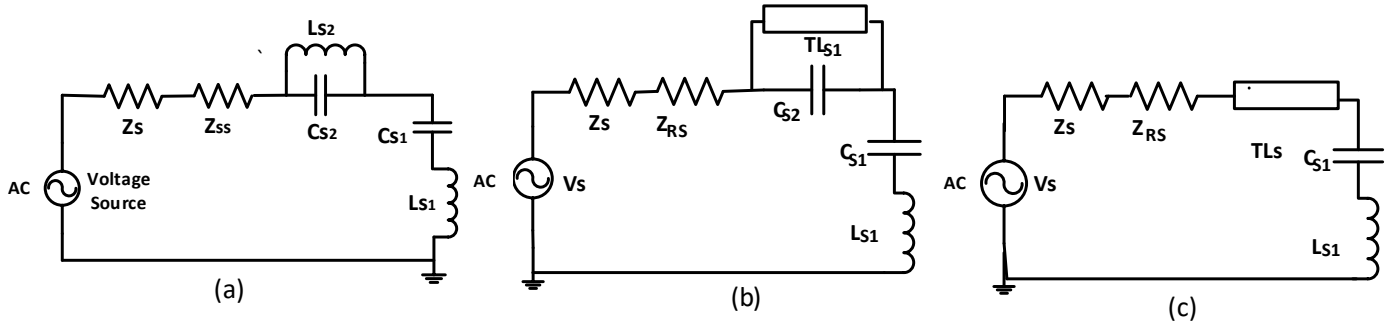

Figure 5. The driver circuit models: (a) Lumped Components, (b) Model 1, and (c) Model 2

FOREX Publication
Open Access | Rapid and quality publishing
International Journal of Electrical and Electronics Research (IJEER)
Research Article | Volume 13, Issue 4 | Pages 772-783 | e-ISSN: 2347-470X

Table 2. Dual-Band Driver Circuit Parameters

Parameter	Unit	Case1			Case2		
		Lumped Components [8]	Model1	Model2	Lumped Components [8]	Model1	Model2
f_{r1}	MHz	6.87	6.87	6.87	6.87	6.87	6.87
f_{r2}	MHz	13.56	13.56	13.56	13.56	13.56	13.56
r_{fr}		2	2	2	2	2	2
r_{fr} /r_{fr}		1.33/0.36	1.33/0.36	1.33/0.36	2/0.5	2/0.5	2/0.5
f_o	MHz	8.83	8.83	8.83	9.588	9.588	9.588
L1	µH	0.564	0.564	0.564	0.564	0.564	0.564
C1	pF	391	391	391	489	489	489
L2	µH	0.317	-----	-----	0.282	------	-----
C2	pF	1086	1086	-----	987	987	------
TL1			Zo =50Ω θ =25°	Zo =16Ω θ =85°		Zo =50Ω θ =25°	Zo =14.5Ω θ =88°

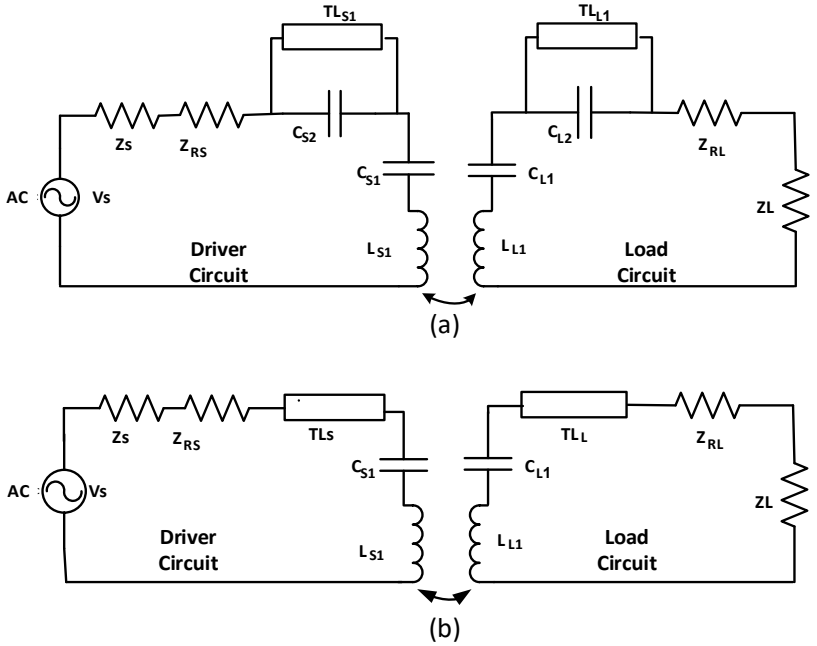

Figure 6. The proposed transmission line equivalent circuit models for Dual-Band complete WPT system: *(a)* Model 1 and *(b)* Model 2

Table 3. Component Value of Dual-Band Complete WPT System

Parameter	Unit	Case3 (Without Matching)				Case4 (With Matching)			
		LC Design1 [7]	LC Design2 [8]	Proposed Model1	Proposed Model2	LC Design1 [7]	LC Design2 [9]	Proposed Model1	Proposed Model2
$_{r1}$	MHz	6.87	6.87	6.87	6.87	6.87	6.87	6.87	6.87
f_{r2}	MHz	13.56	13.56	13.56	13.56	13.56	13.56	13.56	13.56
r_{fr}		f_2	2	2	2	2	2	2	2
r_{fr} /r_{fr}		2/0.5	2/0.5	2/0.5	2/0.5	2/0.5	2/0.5	2/0.5	2/0.5
f_o	MHz	9.588	9.588	9.588	9.588	9.588	9.588	9.588	9.588
L1	µH	1	1	1	1	3	2.8	3	3
C1	pF	275.5	260	275.5	275.5	91.9	100	91.9	91.9
L2	µH	0.5	0.9	-----	-----	1.5	1.3	-----	-----
C2	pF	551.1	550	551.1	-----	183.7	205	183.7	-----
K_{12}		0.18	0.18	0.18	0.18	0.18	0.18	0.18	0.18
TL				Zo =24Ω θ =45°	Zo =30Ω θ =90°			Zo =50Ω θ =25o	Zo =100Ω θ =90°

FOREX Publication
Open Access | Rapid and quality publishing
International Journal of Electrical and Electronics Research (IJEER)
Research Article | Volume 13, Issue 4 | Pages 772-783 | e-ISSN: 2347-470X

4. EXPERIMENTAL SIMULATION RESULTS AND TESTING

4.1. Advance Design System (ADS) Simulation Results

After designing the wireless power transmission models, they had to be tested by simulation using reliable and certified simulation software. Keysight's Advanced Design System (ADS) software was used according to the standards and specifications listed in *table 4*. *Figure 7* illustrates the simulation steps in ADS for simulating the proposed models and displaying the final result. These steps included drawing the circuit to be simulated, selecting the desired motor and simulation type, displaying the results, and calculating the negotiating values that determine the efficiency of the proposed circuit.

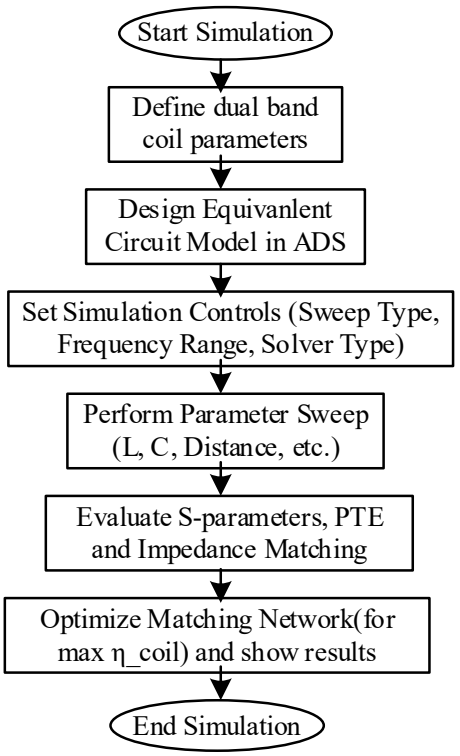

Figure 7. Flow Chart for ADS Simulation Steps

Table 4. ADS Software Parameters

Parameter	Value/Description
Solver Type	S Parameter Simulation / AC Simulation
Frequency Range	0 MHz – 20 MHz
Mesh Type	Adaptive mesh refinement
Boundary Conditions	Open (radiation) boundaries
Convergence Criteria	$\Delta S < 0.001$ between iterations
Port Definition	Two-port network with matched terminations

4.1.1. Dual Band Driver Circuit

Firstly, it is simulated the Dual-Band driver circuits only, which are showed in *figure 3* with its parameters and components value which are listed in *table 2*. *Figure 8* shows the return loss values (S11 in dB) and the imaginary part of the input effective impedance (Ω) for the different inductance ratio (Case 1 and Case 2) listed in *table 2*. The simulation results showed agreement between the previous model and the models proposed in this paper, as expected. The simulation obtained values in *table 5* show the superiority of the two proposed models from previous models and initial agreement with the targeted required.

FOREX Publication
Open Access | Rapid and quality publishing
International Journal of Electrical and Electronics Research (IJEER)
Research Article | Volume 13, Issue 4 | Pages 772-783 | e-ISSN: 2347-470X

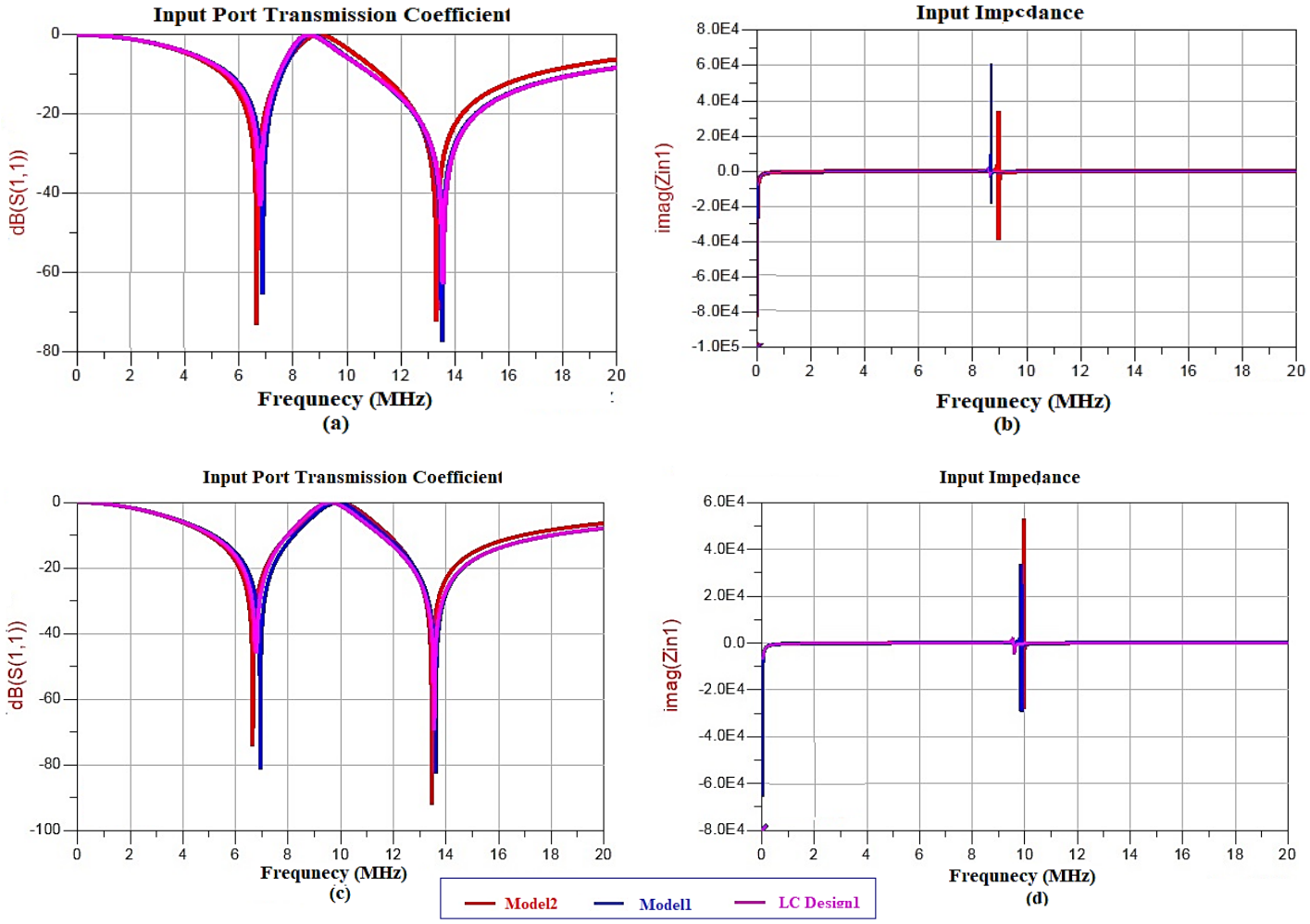

Figure 8. The experimental results of the original and proposed models at the driver circuit in both cases (1) and (2): (a) & (c) reflection coefficient, (b) & (d) Imaginary part of input impedance

Table 5. Experimental Results for Dual-Band WPT Driver Circuit Models

		Case1			Case 2		
Parameter	**Unit**	**LC Design1 [7]**	**Proposed Model1**	**Proposed Model2**	**LC Design1 [7]**	**Proposed Model1**	**Proposed Model2**
f_{r1}	MHz	6.87	6.87	6.87	6.87	6.87	6.87
S_{11} at f_{r1}	dB	-41.688	-29.837	-28.336	-45.613	-29.888	-31.960
Z_{in} at f_{r1}	Ω	0.016	-3.224	3.83	0.074	-3.205	2.524
S_{11} at f_{r1}	dB	-0.434	-0.198	0.088	-0.042	-0.542	-0.660
f_{r2}	MHz	13.56	13.56	13.56	13.56	13.56	13.56
Z_{in} at f_{r2}	Ω	-312.436	-436.562	699.871	-2344.324	341.972	290.167
S_{11} at fr_2	dB	-61.488	-48.651	-31.513	-67.090	-44.369	-37.462
Z_{in} a fr_2	Ω	-0.027	0.369	2.658	-0.732	-1.399	0.405

FOREX Publication
Open Access | Rapid and quality publishing
International Journal of Electrical and Electronics Research (IJEER)
Research Article | Volume 13, Issue 4 | Pages 772-783 | e-ISSN: 2347-470X

4.1.2. Dual Band complete WPT System

Two dual-band wireless power transmission systems, shown in *figure 6* (driver and load circuits together), were also simulated. *figure 9* shows the values of the return loss coefficient (S_{11} in dB), the imaginary part of the input effective impedance (Ω), the forward transfer coefficient (S_{21} in dB), and the PTE value of the coil for the different cases listed in *table 6* (Case 3). The simulation results show that the power received at the load in the dual-band WPT system is significantly greater than that in the single-band WPT system. In some cases, such as the two groups, the received power can be maintained at a relatively high level over a wider range of coupling coefficients. As a result, increasing the coupling coefficient leads to separation, especially at high frequencies. However, the increased PTE at low frequencies is compensated by the decreased PTE at high frequencies. Therefore, a higher receive capacity can be achieved by appropriately balancing different effective separation distances in a dual-band WPT system.

To obtain the maximum power transfer efficiency (PTE), it must be matched to *equation (11)*. The above equation confirms impedance matching for the two-band coil system. A simulation was conducted using the ADS program for all cases. *Table 6* (Case 4) presents the simulation results for the original circuit and the two models proposed in this article for a wireless power transfer system, providing a detailed study of their feasibility and the advantages they offer in reducing unwanted coupling and enabling relatively small circuits. *Figure 10* illustrates the impedance matching achieved in the two models proposed throughout this article. We observe greater matching and improved results, achieving lower coupling at higher resonant frequencies when the same coil size and number of turns are used. Impedance matching at lower-resonant-frequency operation requires strong coupling. When using a lower coil inductance, strong coupling is necessary for impedance matching. If the calculated value of is greater than 1, indicating a non-physical coupling, the coil unit will never achieve impedance matching at these resonant frequencies.

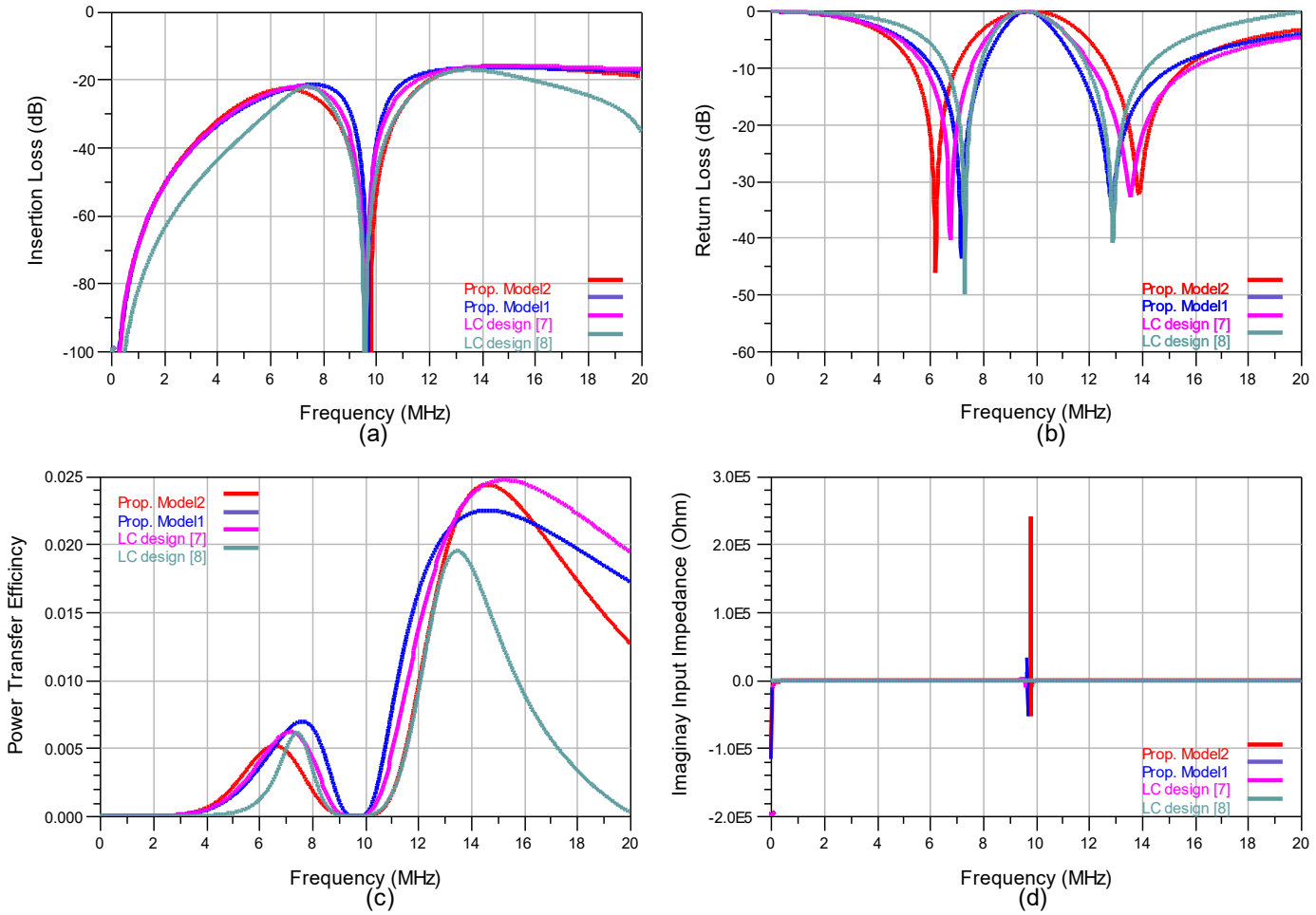

Figure 9. The experimental results of the original and proposed models for case (3): (a) Forward Transmission Coefficient, (b) reflection coefficient, (c) Power Transfer Efficiency & (d) Imaginary part of input impedance

FOREX Publication
Open Access | Rapid and quality publishing
International Journal of Electrical and Electronics Research (IJEER)
Research Article | Volume 13, Issue 4 | Pages 772-783 | e-ISSN: 2347-470X

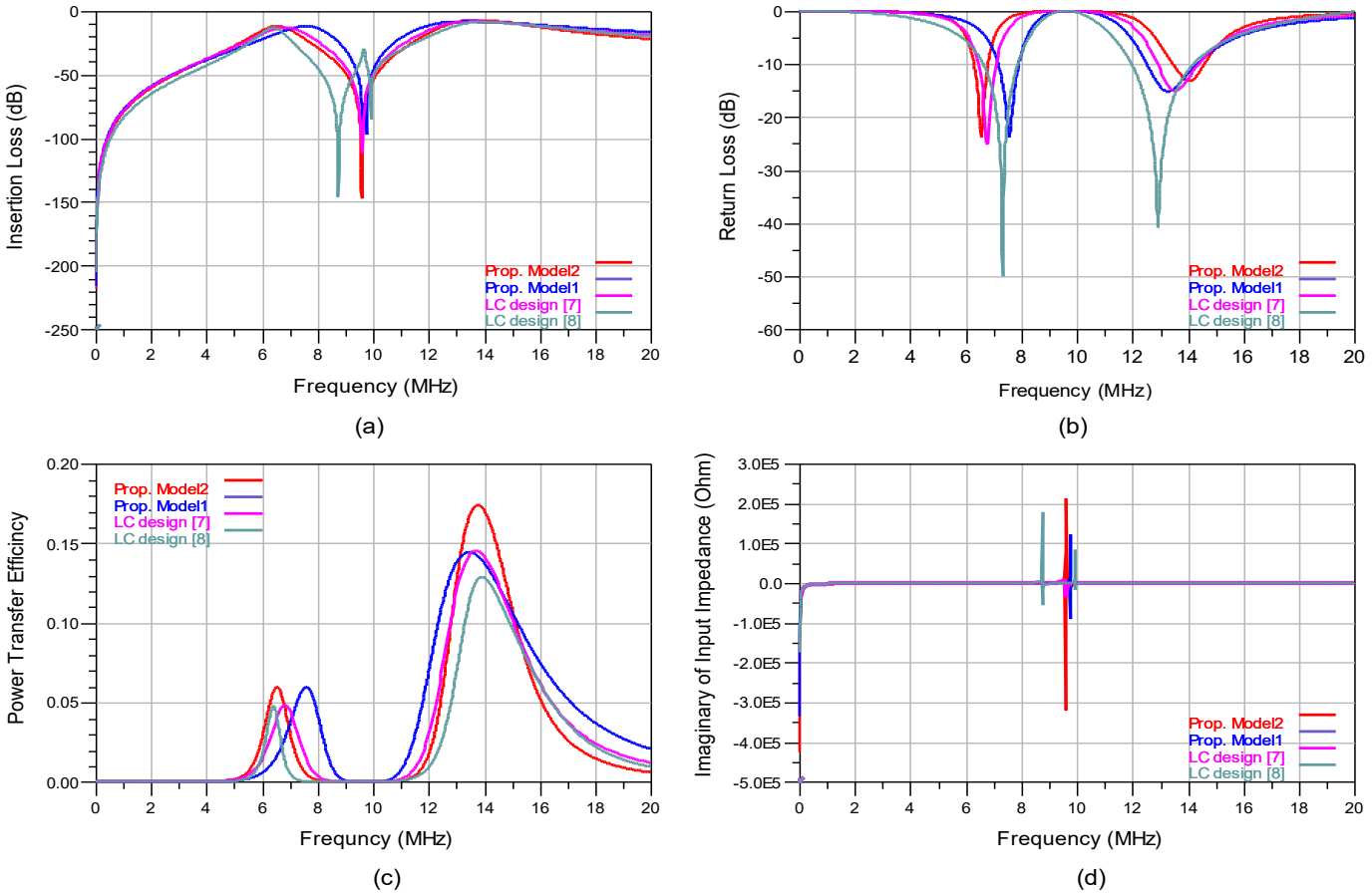

Figure 10. The experimental results of the original and proposed models for case (4): (a) Forward Transmission Coefficient, (b) reflection coefficient, (c) Power Transfer Efficiency & (d) Imaginary part of input impedance

Table 6. Experimental Results for Dual-Band Complete WPT System

		Case3 (Without Matching)				Case4 (With Matching)			
Parameter	**Unit**	**LC Design1 [7]**	**LC Design2 [8]**	**Proposed Model1**	**Proposed Model2**	**LC Design1 [7]**	**LC Design2 [8]**	**Model1**	**Model2**
S_{21} at f_{r1}	dB	-22.358	-24.297	-22.507	-22.495	-13.618	-15.1	-15.040	-14.021
S_{11} at f_{r1}	dB	-39.475	-11.918	-17.702	-17.008	-25.030	-16.13	-7.297	-4.888
Z_{in} at f_{r1}	Ω	0.02	-26.266	-13.002	2.703	0.800	-56.12	-49.638	1.976
PTE at f_{r1}	%	0.6	0.3	0.6	0.5	4.3	3.3	4	5.9
S_{21} at f_o	dB	-64.738	-71.321	-85,923	-66.515	-105.891	-95.3	-73.344	-121.18
S_{11} at f_o	dB	0.120	-0.023	-0.101	-0.001	-0.000007	-0.007	-0.002	-0.00016
Z_{in} at f_o	Ω	-2225.40	-1374.13	5645.46	1241.65	-16782.87	-1165.2	-4218.76	-16298.62
S_{21} at f_{r2}	dB	-16.491	-17.105	-16.615	-16.541	-8.413	-11.54	-10.072	-8.404
S_{11} at f_{r2}	dB	32.717	-15.299	-18.420	-31.263	-15.156	-9.89	-7.599	-14.914
Z_{in} at f_{r2}	Ω	-0.086	15.589	12.140	-0.503	-0.135	-1.45	5.174	-0.782
PTE at f_{r2}	%	2.2	1.6	2.2	2.3	14.5	12.3	14.3	18.2

FOREX Publication
Open Access | Rapid and quality publishing
International Journal of Electrical and Electronics Research (IJEER)
Research Article | Volume 13, Issue 4 | Pages 772-783 | e-ISSN: 2347-470X

4.2. Sodium Adsorption Ratio (SAR) Simulation Results

To simulate the effect of implant tissue loading, we need to model how biological tissue (the implant's environment) affects the WPT system. Given the context, we are likely dealing with a WPT system for biomedical implants, which operates at two frequencies (6.87 MHz and 13.56 MHz). The simulation must account for electromagnetic interactions with lossy, high-permittivity human tissue, which affects the coil's performance (resonance frequency, Q factor, and power transfer efficiency) [19-20]. The SAR (1g, 10g) averaged and checked against safety limits (Use density $\rho \approx 1000$ kg/m³ for tissue, the general formula of SAR is as follows:

$$SAR = \frac{\sigma |E|^2}{2\rho} \quad (10)$$

Where σ represents the conductivity of tissue, E is the delivered energy, and ρ is the mass density. Many tools for simulating SAR, such as High-Frequency Simulation Software (HFSS), are available. If SAR is high or the duty cycle is large, perform a steady-state thermal simulation using a couple of electromagnetic (EM) power deposition terms in the heat equation to predict the temperature rise. Tissue dielectric parameters are as follows:

- Skin: $\varepsilon_r \approx 200–350$ @ 13.56 MHz
- Fat: $\varepsilon_r \approx 10–20$
- Muscle: $\varepsilon_r \approx 250–400$
- Conductivity σ increases with frequency; use frequency-dependent tables.

In this paper, we simulate how the Specific Absorption Rate (SAR) changes in the human body and head when exposed to a magnetic field from a medical wireless system operating in the ISM band (13.56 MHz) with a 1 W input power. A human body model was created using ANSYS HFSS to simulate realistic SAR measurements. The receiver coil was placed inside the human body with a 4mm gap from the transmitting coil, as shown in *figure 11*. It shows the SAR distribution within the head and hand was analyzed by ANSYS HFSS. SAR (Specific Absorption Rate) is commonly defined as the average energy absorbed per unit mass of tissue, typically calculated over 1 gram or 10 grams [20-21]. To safeguard consumer health and safety, international organizations enforce strict standards to ensure products meet established SAR limits. SAR measurement has become a critical factor in assessing product suitability, particularly for medical applications. In this context, a simulated SAR test was conducted on a man's right hand and head, as illustrated in *figure 11*. The study observed the SAR distribution for 1 gram of tissue at 13.56 MHz and 0.22 W/kg. The highest SAR value recorded in the simulation was 0.25 W/kg for one gram of tissue. Notably, the simulated SAR values were well below the maximum thresholds set by international standards for 1 gram of tissue.

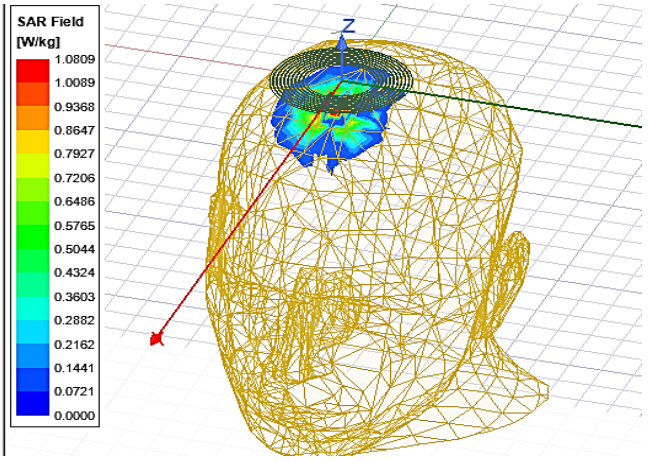

(a)

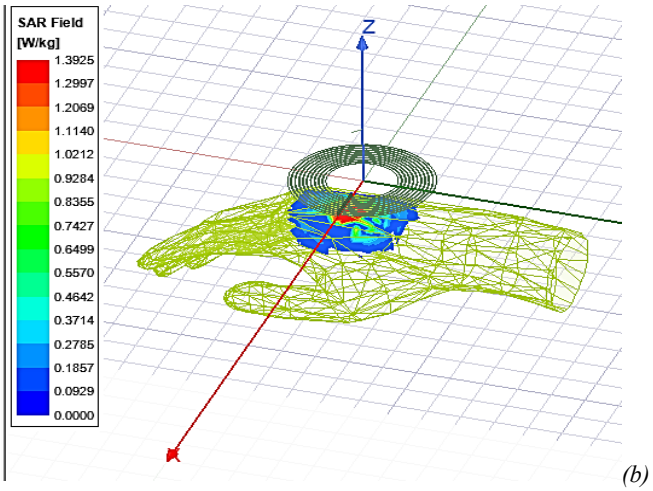

(b)

Figure 11. Experimental Results of SAR Testing: (a) Head tissue and (b) Hand tissue

5. DISCUSSION

To assess the method's efficiency and effectiveness, the two proposed models were tested on the transmission circuit only, as described in the previous paragraph. An integrated wireless power transmission system consisting of both the transmission and reception circuits was then constructed. After that, the two proposed models were tested separately, as shown below. To determine the extent of interaction between the coupling coefficient, impedance ratio, and resonant frequency. Different coil units were used in the original circuit and the two proposed models, listed in *table 3*. The simulation results and the measurement results shown in *figure 9* are consistent. The coil unit with the higher resonant frequency does not require strong coupling to achieve better coil PTE, as shown in the analytical results in *table 6*. Therefore, for a single-band WPT, higher-resonant-frequency operation has a larger coil PTE than lower-resonant-frequency operation when identical coils are used, and the coil separation distance is fixed. This relationship is similar to that of a dual-band coil unit, as shown in *figure 10(c)*. However, higher resonant frequency operation has disadvantages, including reduced PTE due to increase ohmic losses and a smaller near-field reactive region due to the lower

FOREX Publication
Open Access | Rapid and quality publishing
International Journal of Electrical and Electronics Research (IJEER)
Research Article | Volume 13, Issue 4 | Pages 772-783 | e-ISSN: 2347-470X

wavelength. The architecture and its components were experimentally validated, demonstrating high efficiency and flexibility for multi-device WPT scenarios. The model was developed using the proposed method due to its flexibility, and the experimental results closely matched the theoretical predictions. Work is ongoing to improve the design of the data-receiving circuit.

The proposed system offers several benefits, including reduced internal coupling losses. Using distributed transmission-line elements lowers interaction between the two resonant substructures, as shown in *table 7*. More stable PTE over varying coupling distance. Dual-band operation compensates for a drop in PTE at one band when tissue absorption increases at the other. The smaller equivalent component size of TL sections provides the same reactance with higher Q and lower parasitic at the target frequencies.

At its core, the specific security challenge of a dual-band WPT system lies in coordinating two fundamentally different processes (high-power transmission and high-speed data transmission) within a shared space without introducing new risks [20]. Therefore, core safety protocols revolve around intelligent and immediate monitoring and control of the shared electromagnetic environment, ensuring the system remains within strict limits of human exposure and seamlessly shuts down in any failure scenario. Data frequency bandwidth is an integral part of active safety systems. Its use in biomedical applications has made the 6.78 and 13.56 MHz frequencies preferred choices for low-power applications, particularly in near-frequency applications such as surface implants and wearable devices [21]. Electromagnetic wave safety is primarily governed by thermal exposure limits and specific absorption rate (SAR) restrictions, including requirements to prevent interference with other medical devices. Regulatory standards ensure that devices operating at these frequencies remain within safe and biosafety limits.

Table 7. Comparison Table of Dual-Band WPT Systems Characteristics

Reference / Type	Typical PTE	Size / Coil Form	Complexity
Standard Dual-band LC Coil [7].	50–85% (coil-to-coil)	Medium coils; two resonant structures	Low (Simple LC branch + LC tank, but sensitive to parasitics)
Multi-Receiver Dual-Band Coils [8]	70–85% multi-receiver	Larger planar array	High (Supports multiple Rx; complex coupling management)
Proposed TL-Based Dual-Band Coil	improved PTE (60–87%); higher delivered power over a wider coupling range	Compact; TL replaces lumped inductors	Low–Medium (Reduced internal coupling; better performance in multi-coil systems

6. CONCLUSION

This article presents an improved wireless power transmission system model using external inductors with specific inductance values and capacitors, and distributed segments of equivalent transmission lines. This system aims to improve the operation of a dual-band system (6.78 MHz and 13.56 MHz) and reduce inductive coupling resulting from the use of multiple inductors within the circuitry of wireless power transmission systems. The proposed system was tested and validated under various conditions through simulation and experimental results. The simulation results demonstrate the superiority of the proposed power transmission system, achieving high efficiency and effective compatibility with both desired operating frequencies. Key benefits include increased power delivery at resonant frequencies, reduced inductive losses, and improved data transmission rate. An input loss of 8 dB and a low return loss of 14 dB were achieved. Future development will focus on creating a system for simultaneously displaying power and data transmissions and developing a receiver for receiving and displaying the data. A potential application is a mobile wireless charging system that also supports payment services. Although the proposed system demonstrates an improved phase transition coefficient (PTE) (60%) under strong impedance matching and high design flexibility, further development is needed. This includes a practical demonstration of the proposed model, comparison with previous work to measure PTE improvement, and statistical analysis and uncertainty estimation to verify reproducibility.

Nomenclature:

A4WP	Alliance for Wireless Power
C	Capacitor
f_o	Center frequency
f_{ser}	Resonance frequency
ISM	Industrial, Scientific, and Medical
j	Imaginary part
k_{ij}	Coupling factor
L/S	Load/ Source
L_n	Inductor
L_C	Lumped Components
M_B	Mutual inductive
PTE	Power Transfer Efficiency
r	Impedance ratio
R/Z	Resistor / Impedance
RF	Radio Frequency
TL	Transmission Line
X_C	Capacitive impedance
X_L	Inductive impedance
V_S	Voltage Source
ω	Resonance frequency in radian
WPC	Wireless Planning & Coordination
WPT	Wireless Power Transfer
Z_o	Characteristic Impedance
η_{coil}	Power Transfer Efficiency

FOREX Publication
Open Access | Rapid and quality publishing
International Journal of Electrical and Electronics Research (IJEER)
Research Article | Volume 13, Issue 4 | Pages 772-783 | e-ISSN: 2347-470X

Author Contributions: "Conceptualization, authors 1 and 2; methodology, author 1; software, , author 2; validation, authors 1, and 2; formal analysis, author 1 and 2; investigation, author 1; resources, author 2; data curation, , author 1; writing—original draft preparation, author 1; writing—review and editing, author1 and author 2; visualization, author 2; supervision, author 1; project administration, author 1; no funding.

Funding: This research received no external funding.

Conflicts of Interest: The authors declare no conflicts of interest.

REFERENCES

[1] N. Shinohara, *Wireless Power Transfer via Radio Waves*. ISTE–Wiley, 2014.

[2] T. C. Beh, M. Kato, T. Imura, and Y. Hori, "Wireless power transfer system via magnetic resonant coupling at fixed resonance frequency—Power transfer system based on impedance matching," *World Electric Vehicle Journal*, vol. 4, no. 4, pp. 744–753, 2010. [Online]. Available: hflab.ku-tokyo.ac.jp.

[3] M. Simic, C. Bil, and V. Vojisavljevic, "Investigation in wireless power transmission for UAV charging," *Procedia Computer Science*, vol. 6, pp. 1846–1855, 2015, doi: 10.1016/j.procs.2015.08.295.

[4] J. Garnica, R. A. Chinga, and J. Lin, "Wireless power transmission: From far field to near field," *Proceedings of the IEEE*, vol. 101, no. 6, pp. 1321–1331, 2013, doi: 10.1109/JPROC.2013.2251411.

[5] M. Dionigi and M. Mongiardo, "A novel resonator for simultaneous wireless power transfer and near field magnetic communications," in *Proc. IEEE/MTT-S Int. Microwave Symp. Dig.*, 2012, pp. 1–3, doi: 10.1109/MWSYM.2012.6259383.

[6] D. Ahn and P. P. Mercier, "Wireless power transfer with concurrent 200-kHz and 6.78-MHz operation in a single-transmitter device," *IEEE Transactions on Power Electronics*, vol. 31, no. 7, pp. 5018–5029, 2015, doi: 10.1109/TPEL.2015.2480122.

[7] M.-L. Kung and K.-H. Lin, "Enhanced analysis and design method of dual-band coil module for near-field wireless power transfer systems," *IEEE Transactions on Microwave Theory and Techniques*, vol. 63, no. 3, pp. 821–832, 2015, doi: 10.1109/TMTT.2015.2398415.

[8] M.-L. Kung and K.-H. Lin, "Dual-band coil module with repeaters for diverse wireless power transfer applications," *IEEE Transactions on Microwave Theory and Techniques*, vol. 66, no. 1, pp. 332–345, 2017, doi: 10.1109/TMTT.2017.2711010.

[9] S. Mutashar, M. A. Hannan, S. A. Samad, and A. Hussain, "Efficiency improvement of wireless power transmission for bio-implanted devices," *International Journal of Biomedical Engineering*, vol. 7, no. 9, 2013. [Online]. Available: https://www.researchgate.net/profile/Saad-Mutashar/publication/

[10] M.-L. Kung and K.-H. Lin, "A 6.78 MHz and 13.56 MHz dual-band coil module with a repeater for wireless power transfer systems," in *Proc. IEEE Int. Symp. Antennas Propag. (APSURSI)*, 2016, pp. 157–158, doi: 10.1109/APS.2016.7695787.

[11] R. Li and L. Li, "Design of dual-band coil for wireless power transfer system via magnetic resonant coupling," *International Journal of Applied Electromagnetics and Mechanics*, vol. 53, no. 3, pp. 511–521, 2017, doi: 10.3233/JAE-160078.

[12] L. Ji, L. Wang, C. Liao, and S. Li, "Simultaneous wireless power and bidirectional information transmission with a single-coil, dual-resonant structure," *IEEE Transactions on Industrial Electronics*, vol. 66, no. 5, pp. 4013–4022, 2018, doi: 10.1109/TIE.2018.2831196.

[13] M. Liu and M. Chen, "Dual-band multi-receiver wireless power transfer: Architecture, topology, and control," in *Proc. IEEE Appl. Power Electron. Conf. Expo. (APEC)*, 2019, pp. 851–859, doi: 10.1109/APEC.2019.8721837.

[14] A. Fereshtian and J. Ghalibafan, "Impedance matching and efficiency improvement of a dual-band wireless power transfer system using variable inductance and coupling method," *AEU–International Journal of Electronics and Communications*, vol. 116, p. 153085, 2020, doi: 10.1016/j.aeue.2020.153085.

[15] Z. Liu, J. Wang, E. G. Lim, M. Leach, Z. Wang, Z. Jiang, and Y. Huang, "Design of dual-band CPW rectenna for wireless power transmission," in *Proc. Eur. Conf. Antennas Propag. (EuCAP)*, 2024, pp. 1–4, doi: 10.23919/EuCAP60739.2024.10501682.

[16] T. C. Beh, M. Kato, T. Imura, S. Oh, and Y. Hori, "Automated impedance matching system for robust wireless power transfer via magnetic resonance coupling," *IEEE Transactions on Industrial Electronics*, vol. 60, no. 9, pp. 3689–3698, 2012, doi: 10.1109/TIE.2012.2206337.

[17] R. W. Rhea, *HF Filter Design and Computer Simulation*. New York, NY, USA: McGraw-Hill, 1994.

[18] S. Kurokawa, E. C. M. Costa, J. Pissolato, A. J. Prado, and L. F. Bovolato, "Proposal of a transmission line model based on lumped elements: An analytic solution," *Electric Power Components and Systems*, vol. 38, no. 14, pp. 1577–1594, 2010, doi: 10.1080/15325008.2010.492450.

[19] H. K. Abduljaleel, S. K. Gharghan, and A. J. A. Al-Gburi, "Multi-layer square coil-based wireless power transfer for biomedical implants," *Prog. Electromagn. Res. B*, vol. 111, 2025.

[20] S.A.A. Shah, "Empowering the Body: Miniaturized Bioelectronic Devices for Wirelessly-Powered Biotelemetry and Implantation,". *Springer Nature*. 2025.

[21] V. Kumar, S.Gupta, A. Verma, and F.S. Gill. "Specific absorption rate (SAR) in organs of human beings,". In *Challenges in Information, Communication and Computing Technology,* CRC Press, pp. 179-184, 2025.